









Electromagnetically-induced-transparency spectra of Rydberg atoms dressed with dual-tone radio-frequency fields

Maitreyi Jayaseelan ^{1,2,*}, Andrew P. Rotunno ³, Nikunj Kumar Prajapati ³, Samuel Berweger ³,
Alexandra B. Artusio-Glimpse ³, Matthew T. Simons ³ and Christopher L. Holloway ^{3,†}

¹*Department of Physics, University of Colorado, Boulder, Colorado 80302, USA*

²*Associate of the National Institute of Standards and Technology, Boulder, Colorado 80305, USA*

³*National Institute of Standards and Technology, Boulder, Colorado 80305, USA*

 (Received 16 May 2023; revised 21 August 2023; accepted 29 August 2023; published 22 September 2023)

We examine spectral signatures of Rydberg atoms driven with near-resonant dual-tone radio-frequency (rf) fields in the regime of strong driving. We experimentally demonstrate and theoretically model a variety of nonlinear and multiphoton phenomena in the atomic Rydberg response that manifest in the electromagnetically-induced-transparency spectra. Our results echo previous studies of two-level atoms driven with bichromatic optical fields. In comparison to optical studies, the rf-driven Rydberg system utilizes a more complex excitation pathway and electromagnetic fields from two different spectral regimes: a two-photon optical excitation continuously creates highly excited Rydberg atoms, while rf fields drive resonant coupling between the Rydberg levels and generate strong mixing. However, our spectra reflect nearly identical effects of the dual-tone rf fields on the atomic Rydberg observables, showing detuning-dependent splittings and Rabi-frequency-dependent peak numbers and relative strengths, and avoided crossings at subharmonic resonances. We thus validate previous two-state models in this more complex physical system. In the context of Rydberg electrometry, we use these investigations to explore a technique in which we tune a known rf field to observe spectra which give the frequency and power of an unknown rf field using the complex dual-tone spectra.

DOI: [10.1103/PhysRevA.108.033712](https://doi.org/10.1103/PhysRevA.108.033712)

I. INTRODUCTION

Two-level atoms driven by intense bichromatic optical fields have been the subject of extensive experimental [1–4] and theoretical [5–10] investigation. In these systems, both resonance fluorescence and absorption spectra have shown physics beyond the single-frequency Rabi splitting characteristic of atoms subject to monochromatic driving, including detuning-dependent and Rabi-frequency-independent spectral splittings, subharmonic resonances, and phase-dependent atomic dynamics. These investigations point to a wealth of multiphoton dynamics that are accessible to systems driven by multiple frequencies: bichromatic electromagnetically induced transparency (EIT) has been demonstrated in both cold atoms [11] and hot vapors [12], and bichromatic and multifrequency fields have been employed in novel cooling methods for alkali atoms [13]. Looking beyond atomic vapors, the spectra of bichromatically driven solid-state systems with single-molecule impurities [14] and nuclear spins of nitrogen vacancy centers in diamond [15] have revealed well-resolved subharmonic resonances and multiphoton effects, while a bichromatically driven quantum-dot system demonstrated predicted quantum interference effects in fluorescence spectra [16,17].

In the radio-frequency (rf) and microwave domains [megahertz (MHz) and gigahertz (GHz)], dual-tone dressing has been used to demonstrate a dynamically modulated Autler-Townes (AT) effect in superconducting qubits, providing an enhanced experimental toolbox for qubit manipulation and control [18]. It has also been investigated in the context of alignment-based magnetic resonance spectra in cesium, where dual-tone driving between the ground-state hyperfine levels modifies the standard AT splitting of the system dressed by a single field [19]. In Rydberg atoms, dual-tone microwave dressing was used to achieve a polarizability nulling effect [20]. An aspect of Rydberg systems that has been less explored is their behavior under near-resonant dual- and multitone rf dressing.

Over the last decade, continuously detected Rydberg EIT systems have proven to be an invaluable technology for sensitive, external calibration-free electrometry using the AT splitting (Rabi splitting) of Rydberg energy levels dressed by an rf field [21]. Under single-tone resonant driving, the AT spectra display splittings proportional to field strength, providing a direct measurement of electric field; the number and relative strengths of spectral peaks are independent of field strength in this case. For strong driving with dual-tone rf dressing, multiphoton effects may be expected to yield spectra that are qualitatively different from those obtained with single-tone driving.

Here, we extend the physics of bichromatic optical dressing of atoms to the rf regime, using a two-level Rydberg system probed by EIT in a warm atomic vapor of ⁸⁵Rb. The

*maitreyi.jayaseelan@colorado.edu

†christopher.holloway@nist.gov

atomic population is driven from the ground electronic state into a Rydberg state via an intermediate energy level using a two-photon optical excitation scheme that employs independent probe and coupling laser fields. We observe the EIT of the probe laser field that appears due to a combination of ac Stark splitting due to the coupling field and interference in the decay of the dressed atomic levels [22–24]. Two near-resonant rf fields couple this Rydberg state to an adjacent Rydberg state. While the full dynamics of this system is rather complex, we show that the experimental spectra may be modeled more simply by treating the two Rydberg levels as an isolated two-level system driven by a dual-tone electromagnetic field. We use a Floquet analysis to model the response of the dressed Rydberg levels, obtaining good agreement with the rich experimental spectra.

We emphasize that the experimental spectra are optically detected (EIT) Rydberg-state energy spectra. The two-level dressed-atom physics of the rf-Rydberg system is probed with electromagnetic frequencies belonging to a spectral range different from those fields that create the multiphoton Floquet spectra. Our results thus validate the applicability of two-level dressed-atom physics in the rf domain, where the optical fields that create the highly excited Rydberg atoms may in turn be regarded as indirect probes that do not significantly alter the relatively long-lived two-level system dynamics. Since the Rydberg system displays a wide range of resonances from GHz to MHz frequencies, these models may be validated for a wide range of dressing-field frequencies. Further, the large electric dipole moments of highly excited Rydberg states allow the multiphoton dynamics of dual-tone dressed atoms to be demonstrated with modest rf field amplitudes when compared to optical dressing.

We distinguish our experiments from the “atom-mixer” configurations which used two rf tones applied to the atoms to transfer an intermediate frequency into the optical domain, providing phase-sensitive detection for rf fields [25]. The atom mixer used a strong resonant local oscillator and a weaker signal field several kilohertz (kHz) detuned and well within the EIT linewidth. Further, only the resulting beat signal on the optical frequency of the probe was detected. Here, we operate in the strong-driving regime, where both rf fields contribute nontrivially to the multiphoton dynamics that are integral to the spectra we observe. We explore configurations in which one or both fields are far ($\lesssim 200$ MHz) off resonance from the Rydberg transition. We further distinguish these experiments from previous bichromatic EIT configurations [11,12] that used optical fields in a three-level Λ configuration in contrast to our experiment, where the dual-tone rf-induced Rabi splitting of two Rydberg levels is probed by a cascade EIT system, and from the dual-tone driving of atomic energy levels employed in Ref. [19], where the coupling is through the magnetic dipole term.

We begin with a description of the experimental Rydberg EIT setup in Sec. II and present our dual-tone two-level Floquet theoretical model in Sec. III. Experimental results are compared with computed spectra in Sec. IV for “symmetric” cases and “asymmetric” cases in Sec. V, with an eye toward applications. We conclude in Sec. VI. Extensions of our model to include atomic fine structure and magnetic structure are given in the Appendix.

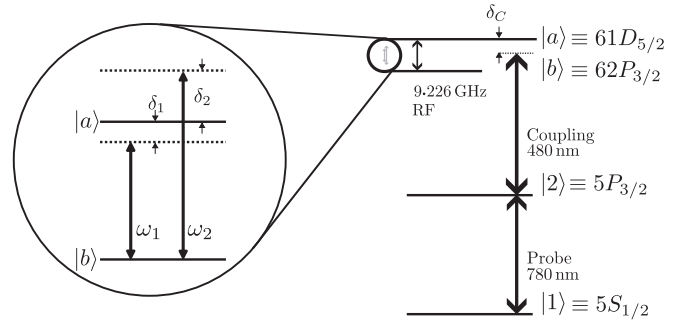


FIG. 1. Rydberg atom with applied dual-tone rf fields.

II. EXPERIMENT

We use a two-photon excitation scheme to create excited Rydberg atoms in a ^{85}Rb vapor cell at room temperature. The excitation pathway $5S_{1/2} \rightarrow 5P_{3/2} \rightarrow nD_{5/2}$ is shown in Fig. 1. We use a probe laser at 780 nm, locked to the $F = 3 \rightarrow F' = 4$ transition on the D_2 line of ^{85}Rb , and a counter-propagating coupling laser at 480 nm to excite atoms into the Rydberg state. We employ cascade EIT between the atomic ground state and the Rydberg state as our detection scheme: as the coupling laser is scanned through the Rydberg manifold, EIT of the probe beam appears when the two-photon system is resonant with a Rydberg state. Both lasers are power locked with acousto-optic modulators. We isolate the EIT signal using differential detection of two power-balanced probe beams; one beam overlaps with the coupling laser for EIT, and the other provides an absorption reference.

In this experiment, we investigate the response of the atomic Rydberg states to a dual-tone rf field addressing the Rydberg transition $61D_{5/2} \rightarrow 62P_{3/2}$ with transition dipole moment $\wp = 2366ea_0$ and a resonant transition frequency of 9.226 GHz, calculated using the ARC software package [26]. The Rydberg transition resonance frequency ω_0 is verified using a single rf field at moderate power and balancing the two AT split peaks. The rf fields are applied to the vapor cell using a horn antenna that is oriented such that the rf fields propagate perpendicular to the direction of propagation of the optical fields. The rf fields and the probe and coupling lasers are all linearly polarized in the \hat{z} direction, perpendicular to the plane of the optical table. The two rf tones whose effects we investigate in this work are outputs from a dual-output signal generator with independently controllable powers and detunings. The two outputs are combined with a power combiner and applied to the rf horn antenna. The two rf tones are phase coherent when both are at the same frequency, and the amplitude depends on the constant, but arbitrary, relative phase between the two outputs. When different frequencies are combined, the phase evolves at the beat-note frequency.

For our data, we use a frequency scale set by a scan of the coupling laser detuning δ_c over the states $61D_{3/2}$ and $61D_{5/2}$, which have a fine-structure splitting of 50.339 MHz, calculated using Ref. [26]. These EIT scans, simultaneously collected in a reference cell away from the horn, also provide a frequency reference to correct for offsets of the scans due to laser drift and other environmental effects. A slight residual “drift” toward negative δ_c is observed with increased field,

potentially as a result of residual field-dependent shifting in the reference cell, which was poorly shielded from rf reflections. The two-level theory that we employ does not reproduce these shifts; however, the spectral characteristics we emphasize in this work remain unaffected.

III. THEORETICAL FRAMEWORK: FLOQUET HAMILTONIAN

We now discuss a simplified theoretical model that we will use to analyze our experimental data. We restrict this discussion to the dynamics of a two-level atomic system composed of two Rydberg states dressed by a dual-tone rf field. The two-level model reproduces the main features of the experimental spectra with good agreement, which is one of the main results of this work. Extensions to the two-level model that consider atomic structure are discussed in the Appendix.

Consider two Rydberg states $|a\rangle$ and $|b\rangle$ dressed with a dual-tone rf field of the form

$$\mathbf{E}(t) = [|E_1| \cos(\omega_1 t) + |E_2| \cos(\omega_2 t + \Phi)] \hat{\mathbf{z}}, \quad (1)$$

where $|E_i|$ is the magnitude of the field at frequency ω_i and Φ is the relative phase between the two fields. We denote the bare Rydberg atomic resonance as ω_0 , so that $\delta_1 = \omega_0 - \omega_1$ and $\delta_2 = \omega_0 - \omega_2$ are the detunings of the two field components from the Rydberg resonance. We note that the trigonometric identity

$$\cos(\theta) + \cos(\phi) = 2 \cos\left(\frac{\theta + \phi}{2}\right) \cos\left(\frac{\theta - \phi}{2}\right)$$

suggests the interpretation of our dual-tone setup as a carrier at the mean frequency, amplitude modulated at a rate of half their difference.

Defining the Rabi frequencies of the two components as $\Omega_i = -\langle a | \mathbf{d} \cdot \hat{\mathbf{z}} | b \rangle |E_i| / \hbar$, where $\varrho_{a,b} = \langle a | \mathbf{d} | b \rangle$ is the atomic dipole moment and $\hat{\mathbf{z}}$ is the direction of linear polarization of the applied rf fields, the interaction Hamiltonian in the rotating-wave approximation (RWA) is [27]

$$H_{\text{RWA}} = \frac{\hbar}{2} \begin{pmatrix} 0 & \Omega_1 e^{-i\delta_1 t/2} + \Omega_2 e^{i(\delta_1 t/2 + \Phi)} \\ \Omega_1^* e^{i\delta_1 t/2} + \Omega_2^* e^{-i(\delta_1 t/2 + \Phi)} & -\Sigma_\delta \end{pmatrix},$$

where we define the difference and sum of the two rf detunings $\delta_{1,2}$:

$$\delta_\delta \equiv \delta_2 - \delta_1 = \omega_2 - \omega_1, \quad (2)$$

$$\Sigma_\delta \equiv \delta_1 + \delta_2 = 2\omega_0 - (\omega_1 + \omega_2). \quad (3)$$

We set $\Phi = 0$ in the subsequent analysis. Note that setting $|\Omega_1| = |\Omega_2|$ reduces H_{RWA} to the laboratory-frame Hamiltonian of a two-level system with energy separation Σ_δ coupled by a field at frequency $\delta_\delta/2$. A particular case is for $\delta_1 = -\delta_2$, where the Floquet modulation frequency is equal to the detunings, $\delta_\delta/2 = |\delta_1| = |\delta_2|$, and in the RWA the states are degenerate because $\Sigma_\delta = 0$.

Unlike the case of a two-level atom dressed by a monochromatic field, the dual-tone dressed system in the rotating frame shows a residual time dependence in the off-diagonal coupling

terms, so that the Schrödinger equation for the system cannot be integrated directly. Nevertheless, the time periodicity of the residual driving confers a symmetry that allows a conserved quasienergy for the system. We treat this residual time dependence using a Floquet picture, following Shirley's approach to obtaining the Floquet modes and quasienergies of the periodically modulated system [28]. This approach promotes the time-dependent Hamiltonian from the state space \mathcal{H} to an extended Floquet space where the eigenvectors are now labeled by two indices: the eigenindex of the bare Hamiltonian and the "photon-number" index of the Floquet mode of N photons with a frequency at the Floquet frequency ($\omega_F \equiv \delta_\delta/2$). In this extended space, the harmonic components of the Schrödinger eigenvalue equation obey a recursion relation:

$$\begin{pmatrix} 0 & 0 \\ 0 & -\Sigma_\delta/2 \end{pmatrix} \begin{pmatrix} a_N \\ b_N \end{pmatrix} + \begin{pmatrix} 0 & \Omega_1/2 \\ \Omega_2^*/2 & 0 \end{pmatrix} \begin{pmatrix} a_{N+1} \\ b_{N+1} \end{pmatrix} + \begin{pmatrix} 0 & \Omega_2/2 \\ \Omega_1^*/2 & 0 \end{pmatrix} \begin{pmatrix} a_{N-1} \\ b_{N-1} \end{pmatrix} = (\epsilon + N\hbar\omega_F) \begin{pmatrix} a_N \\ b_N \end{pmatrix}. \quad (4)$$

In the dressed-state basis and for equal Rabi frequencies $|\Omega_1| = |\Omega_2| = |\Omega|$, the ladder of states separated by the Floquet frequency ω_F has a tridiagonal representation that leads to a Bessel-function representation $d_N \propto J_N(\Omega/\omega_F)$ within a dressed-state manifold, where d_N are the expansion coefficients of the atom-field coupled dressed states in the bare-state basis [7].

Using Eq. (4), we may build an infinite-dimensional time-independent Floquet Hamiltonian \mathcal{H}_F that satisfies the eigenvalue equation $\mathcal{H}_F \boldsymbol{\varphi}_N = \epsilon_N \boldsymbol{\varphi}_N$. In practice, the infinite-dimensional Hamiltonian is truncated to some large value N_{max} for which the solutions converge. All two-level models in this work use $N_{\text{max}} = 50$, which was more than sufficient for reasonable convergence. An example cutoff criterion is that the population in the N_{max} th sideband is small, i.e., $< 0.1\%$ of the population.

We obtain the eigenvectors and eigenenergies by diagonalizing the Floquet Hamiltonian \mathcal{H}_F . These eigenvectors and eigenenergies are the Floquet modes and quasienergies ϵ_N , represented in the expanded Floquet basis. To compute the Floquet-mode occupation given a specific input state, we project the initial state into the Floquet basis and compute the square of these amplitudes [28]. We plot the mode occupation against quasienergy ϵ to generate the theory waterfall plots. The Floquet modes and quasienergies are sensitive to the detunings and the individual Rabi frequencies of the applied rf fields. In this work, we examine the spectral signatures of the Rydberg response as these parameters are varied.

IV. EXPERIMENTAL RESULTS: SYMMETRIC DETUNING AND POWER-BALANCED FIELDS

Our main results are the observed agreement between experimental Rydberg EIT spectra and a theoretical model of the dual-tone driven Rydberg system. We predict and observe many nonlinear and multiphoton effects due to the dual-tone rf dressing.

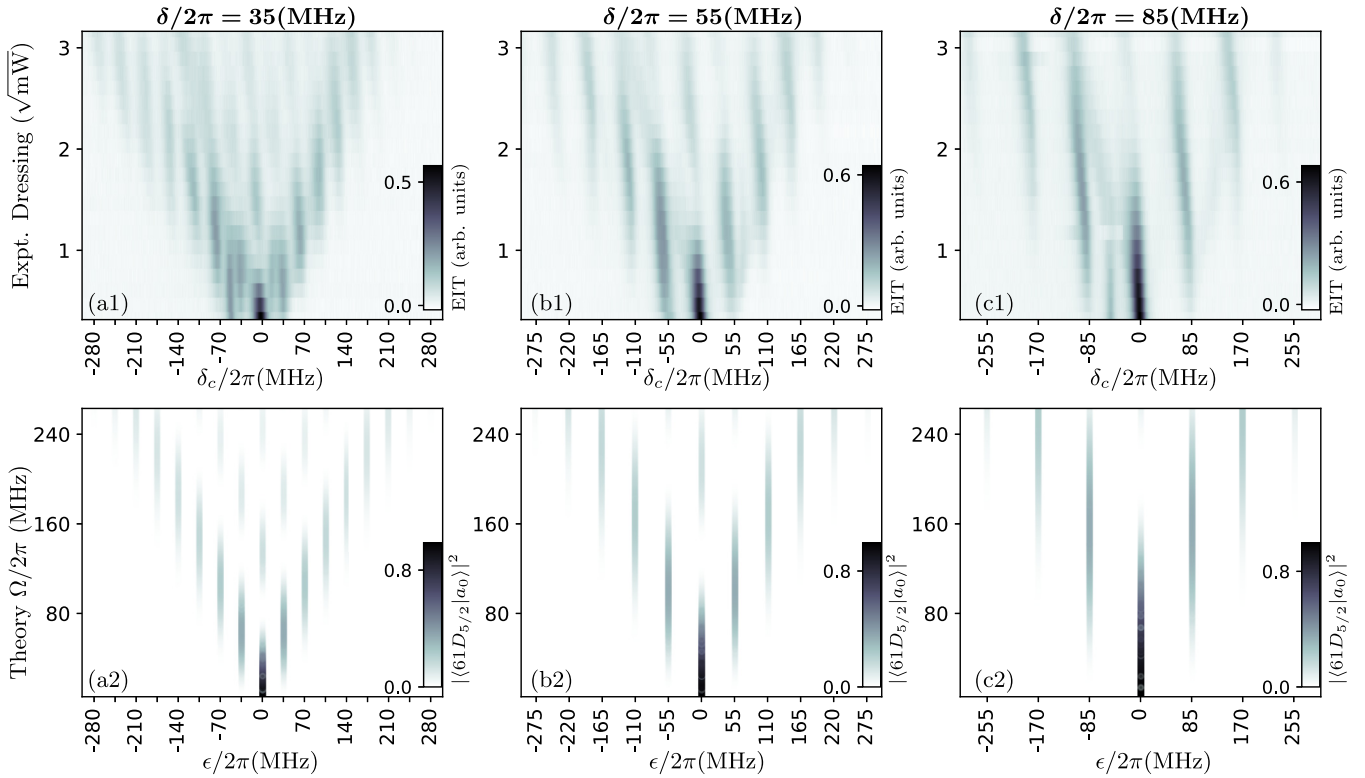


FIG. 2. (a1)–(c1) Experimental and (a2)–(c2) theoretical waterfall plots showing Rydberg EIT spectra obtained through a simultaneous scan of $|\Omega_1| = |\Omega_2| = |\Omega|$ with detunings $\delta_1 = -\delta_2 = \delta$ kept constant. The spectral features appear at coupling laser detunings spaced by the symmetric detuning δ . The columns correspond to $\delta = 35, 55,$ and 85 MHz, from left to right. These locations are marked on the x axis to emphasize the appearance of the spectral peaks at these locations. The features are reproduced in the theoretical Floquet quasienergy spectra, with waterfall plots over Ω showing the mode occupations of Floquet modes against Floquet quasienergy ϵ . The Floquet modes appear at quasienergies spaced by δ , and this spacing remains constant as we scan Ω . The mode occupation has a sensitive dependence on Ω .

We present experiment alongside theoretical predictions, using similar axes with different units, matching experimental and theory parameters. The energy spectrum is scanned experimentally by laser detuning δ_c , and state theory energy is given in units of the quasienergy ϵ . The color or darkness axis represents experimental transmittance (EIT), alongside theory population projections of the $61D_{5/2}$ state into the Floquet modes. The waterfall axis scans applied field strength in $\sqrt{\text{mW}}$, pairing with Rabi frequencies Ω . We convert between Rabi frequency and applied field with a two-point function using Rabi frequencies of $2\pi \times \{70, 160\}$ MHz for applied rf powers of $\{0.24, 6.12\}$ dBm (or rf field strengths of $\{1.03, 2.02\} \sqrt{\text{mW}}$), which agrees well with the experimental data and corresponds to a linear region of a single-field Autler-Townes scan of Rabi frequencies. We compensate the powers sent to the horn to maintain field strength ($\sqrt{\text{mW}}$ or $|\Omega|$) across the horn’s frequency-dependent gain curve.

In the following sections we discuss the spectral features of experimentally obtained EIT spectra for a variety of configurations of rf fields. The main features of our experimental spectra are very well modeled by a simple two-state Hamiltonian that includes just the Rydberg states $61D_{5/2}$ and $62P_{3/2}$, coupled with a linearly polarized dual-tone rf field. In this section, we demonstrate the effect of applied symmetric rf dual-tone fields that are symmetrically detuned ($\delta_1 = -\delta_2 = \delta$) from the Rydberg resonance frequency of 9.226 GHz and

power balanced, with equal Rabi frequencies ($|\Omega_1| = |\Omega_2| = |\Omega|$). In Sec. IV A, we scan the Rabi frequency Ω for a few fixed detunings δ , and in Sec. IV B, we scan the detuning δ for a few fixed Rabi frequencies Ω .

A. Scanning Rabi frequencies

Our first set of results is presented in Fig. 2, which shows waterfall plots of Rydberg EIT spectra as the symmetric detuning δ is held constant while both power-balanced Rabi frequencies $|\Omega|$ are simultaneously scanned. We present data for three different values of δ .

For this case, the two-state model predicts equal and opposite energy shifts of the states at each Rabi frequency; the eigenvalues of the Floquet Hamiltonian are equal to the elements on the diagonal. The quasienergies therefore remain unchanged as the Rabi frequency is scanned, resulting in spectra in which the spacing of the Floquet modes is set entirely by the detunings, and this mode spacing remains constant as Rabi frequencies are swept.

The Floquet-mode occupation is, however, sensitive to the Rabi frequencies: higher Rabi frequencies populate modes with higher photon numbers. The mode occupations follow the Bessel functions in this two-state model (the inclusion of more states causes deviations from this Bessel-function behavior): $d_N \propto J_N(\Omega/\delta)$, where N signifies the Floquet-mode index and Ω and δ are the balanced Rabi frequencies and

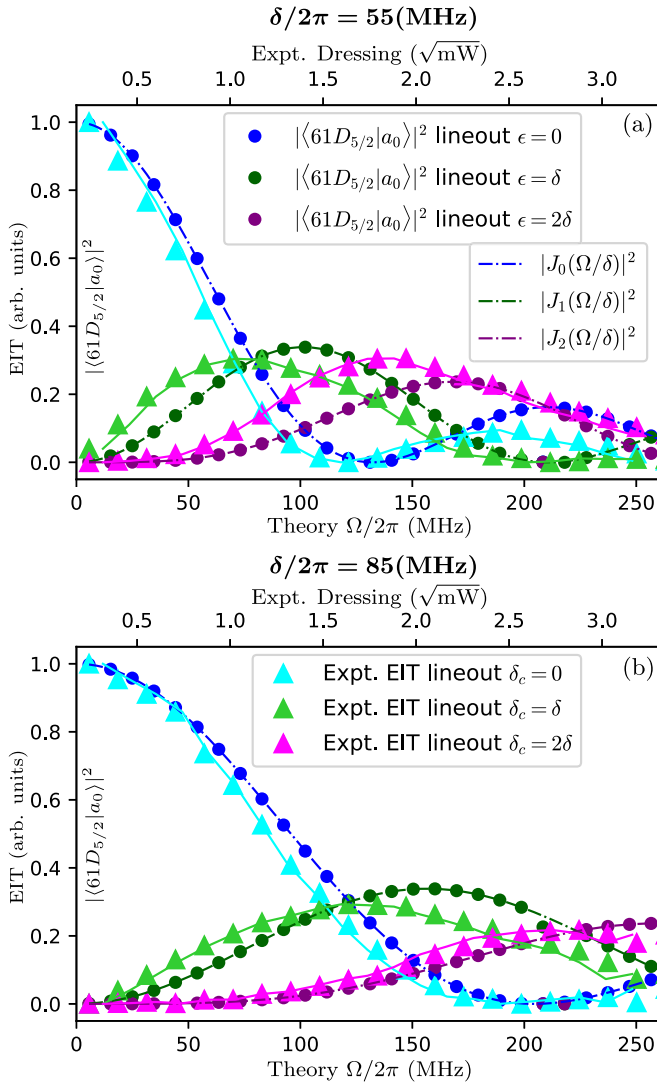


FIG. 3. Bessel-function form of the mode occupation and corresponding EIT peak height for symmetrically detuned fields as the power-balanced Rabi frequencies are simultaneously scanned. (a) shows the line-outs (profile along the line) of the first three Floquet modes for $\delta = 55$ MHz. We show the numerically computed mode occupations at intervals (circles) superposed on analytic Bessel functions (dash-dotted lines). In the same plot we show the experimentally obtained EIT peak heights (triangles), which are connected by lines to guide the eye. Blue, green, and purple elements in the plots depict the zero-, first-, and second-order Floquet modes. (b) shows the same line-outs for $\delta = 85$ MHz.

symmetric detunings of the two rf tones [7]. The Bessel functions are visually represented in the data in Fig. 2, as seen by following the peak heights corresponding to a specific value of detuning δ as we scan the dressing-field power (that is, looking at a vertical slice of a waterfall plot at the locations $\delta_c = N\delta$).

In Fig. 3 we demonstrate the good agreement of a theoretical Bessel-function form with line-outs of vertical slices of the experimental and theoretical waterfall plots in Figs. 2(b) and 2(c). We plot the closed-form Bessel functions for direct comparison. For our two-state model, we see that the numerical

computation matches up exactly with the analytic functional form. The experimental line-outs are computed as an average over a small window of frequencies (ϵ or δ_c), compensating the leftward drift with a linear shift of the averaging window with Rabi dressing. In our data, we see that the experimental line-outs map well to the numerical and analytic values for the Bessel functions. We attribute small deviations of the experimental lines from the analytic expression to experimental factors, including the presence of nearby atomic resonances and uncertainties in the mapping between theoretical and experimental Rabi frequencies.

We note that the original investigations of bichromatic optical driving of two-level atoms showed distinct linewidths for the odd and even Floquet modes; these widths were later shown to depend on the ratio of the Rabi frequency to the Floquet frequency ($\delta_\delta/2$), as well as the natural widths of the atomic states [7]. In our data, the two Rydberg levels have very similar decay rates and state decay linewidths in the kHz regime—the state lifetimes at room temperature, computed using Ref. [26], are $\tau_{61D_{5/2}} \approx 110 \mu\text{s}$ and $\tau_{62P_{3/2}} \approx 145 \mu\text{s}$ —and we observe no obvious difference in the linewidths of the even and odd peaks, which are primarily set by the Doppler-broadened EIT linewidth (typically several MHz).

B. Scanning detunings

Our second set of results is presented in Fig. 4, which shows waterfall plots of Rydberg EIT spectra as the power-balanced equal Rabi frequencies of the two fields are constant while the symmetric detunings $\delta_1 = -\delta_2 = \delta$ are simultaneously scanned. We present data for three different values of Ω . We note that the spectra are primarily visible in the range $-\Omega < \delta_c < +\Omega$.

Again, the symmetric detunings each produce equal and opposite energy shifts of the states, and the eigenvalues of the Floquet Hamiltonian are determined by its diagonal elements. These eigenvalues are thus spaced by multiples of the Floquet frequency $\omega_F \equiv \delta_\delta/2$. The mode spacing changes linearly over the waterfall plot with detuning—this is in contrast to Fig. 2, where the constant detunings (labeled in each plot) result in equal-spaced spectral features over the waterfall with Rabi frequency.

Here, we see that for the three different values of the Rabi frequency the behavior of the quasienergies with detuning remains the same. However, higher Rabi frequencies drive population to higher-order Floquet modes, resulting in a larger fanning out of the spectra; note the different scales of the color maps for the three cases, as population is spread out among a greater number of Floquet modes. The Bessel functions determining the mode occupation, $d_N \propto J_N(\Omega/\delta)$, are less visually apparent in these spectra because the denominator of the Bessel-function argument changes over the waterfall.

An important aspect of Rydberg systems is the strong interaction between Rydberg atoms. For resonant microwave dressing, an enhanced blockade effect can modify or suppress the EIT signal even for weak microwave powers [29]. This places a limit on the minimum detuning δ , which scales with the microwave power, beyond which (closer to resonance) interaction effects play a larger role; these effects may contribute to the appearance of the spectra close to $\delta = 0$.

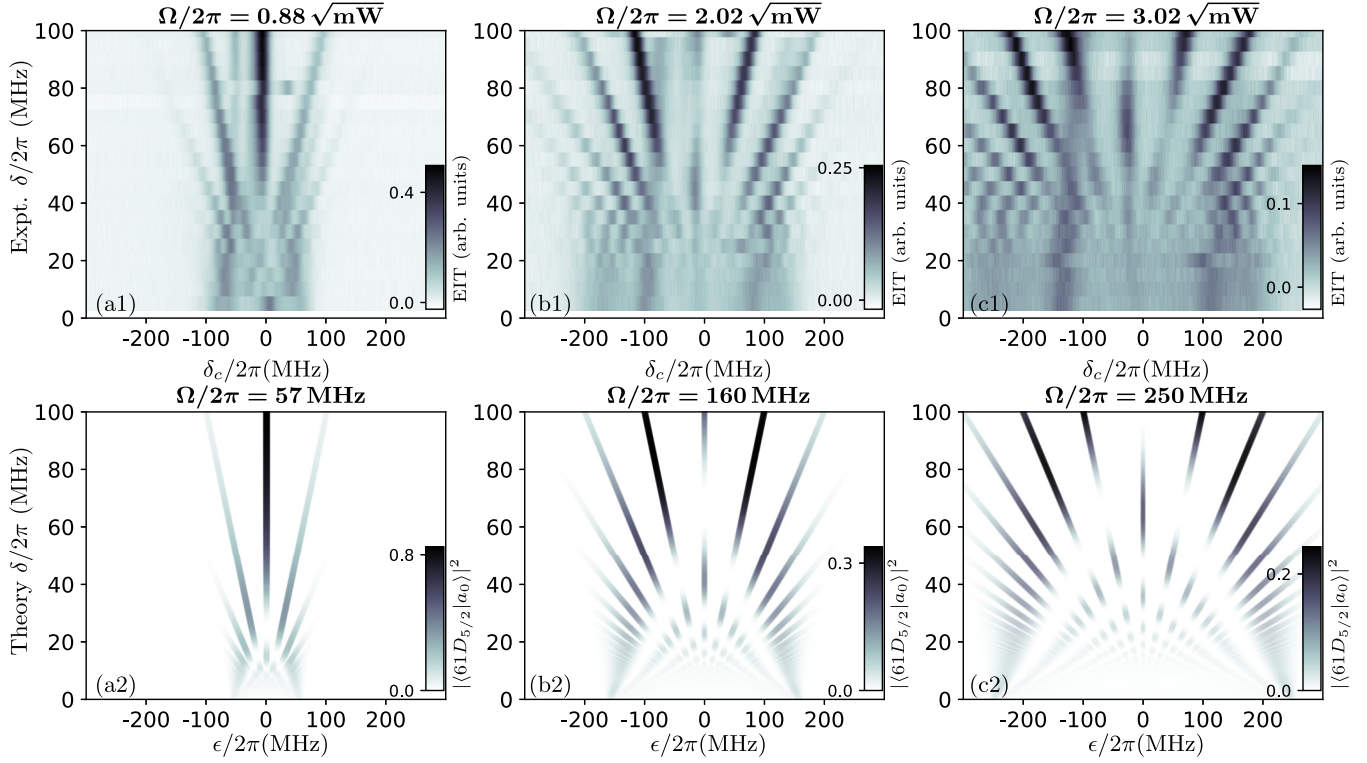


FIG. 4. (a1)–(c1) Experimental and (a2)–(c2) theoretical waterfall plots showing a simultaneous scan of $\delta_1 = -\delta_2 = \delta$ while the two Rabi frequencies $|\Omega_1| = |\Omega_2| = \Omega$ are kept constant. The mode quasienergies are shown to increase with δ in each waterfall plot, and the splitting between the Floquet modes is linear in δ for the range of Ω shown. Increasing the Rabi frequency has the effect of populating Floquet modes with a higher Floquet photon index. At higher driving Rabi frequencies we see an overall shift of the spectra toward lower energy [as seen in (c1)]. We attribute this shift to imperfect shielding of our reference cell from the applied rf fields.

V. APPLICATION SCENARIO: ASYMMETRIC AND UNBALANCED FIELDS

With an eye toward application scenarios, we consider the case where one field parameter is held and the other controlled field is swept in power or detuning while we observe the dual-tone Rydberg EIT spectrum. We note that any particular spectrum can give information about both tones; moreover, if one can “tune” into the symmetric and balanced cases, the known field strength and frequency can give the “unknown” rf signal’s parameters. We illustrate here trends which appear as one moves away in either asymmetric-detuning or unbalanced-power scenarios.

In Sec. IV A we demonstrated the dependence of the symmetric dual-tone spectra on detuning and Rabi frequency. The quasienergies remain constant with Rabi frequency for symmetric detunings and unbalanced Rabi frequencies. In general, the spectra are more complex functions of these parameters. For instance, for asymmetric detunings or Rabi frequencies, the quasienergies oscillate as the symmetric Rabi frequencies are simultaneously scanned. The spectra in Figs. 2 and 4 offer a tool for characterizing an unknown rf frequency through frequency and power matching with scans of the Rabi frequencies and detuning.

A. Unbalanced power with symmetric detuning

Our third set of results is presented in Fig. 5, which shows waterfall plots of Rydberg EIT spectra for unbalanced, but

constant, Rabi frequencies as the symmetric detunings $\delta_1 = -\delta_2 = \delta$ are simultaneously scanned. In these plots, $|\Omega_2| = 1\sqrt{\text{mW}}$ was held constant, and we present data for five different values of $|\Omega_1|$. The mismatched Rabi frequencies cause an asymmetric spectrum in which the shift is indicative of the relative Rabi frequencies. A similar behavior can be observed for mismatched detunings. These asymmetric spectra thus allow a determination of the detuning of an unknown rf field based on the symmetry of the quasienergy curves.

At low values of Ω_1 as in Figs. 5(a) and 5(b), the plots resemble one half of an avoided crossing as the stronger Ω_2 field moves off resonance forming a few visible avoided crossings. When $\Omega_1 = \Omega_2$, as in Figs. 5(c1) and 5(c2), the features represent the prior symmetric case and illustrate a “tuning in” of the balanced-power condition. When $\Omega_1 > \Omega_2$, as in Figs. 5(d) and 5(e), we observe additional significant avoided crossings due to both fields, as the system trends toward the strong avoided crossing from Ω_2 with detuning opposite that in Fig. 5(a). These data also demonstrate a key feature of this experimental system, that EIT-accessible states appear within $-\Omega_{1,2} < |\delta_C| < \Omega_{1,2}$ of the original EIT resonances.

B. Asymmetric detuning with balanced power

Our final set of results is presented in Fig. 6, which shows waterfall plots of Rydberg EIT spectra in which the equal Rabi frequencies of the two fields and the detuning δ_2 are held constant while δ_1 is swept through the resonance. We present data for seven different values of δ_2 .

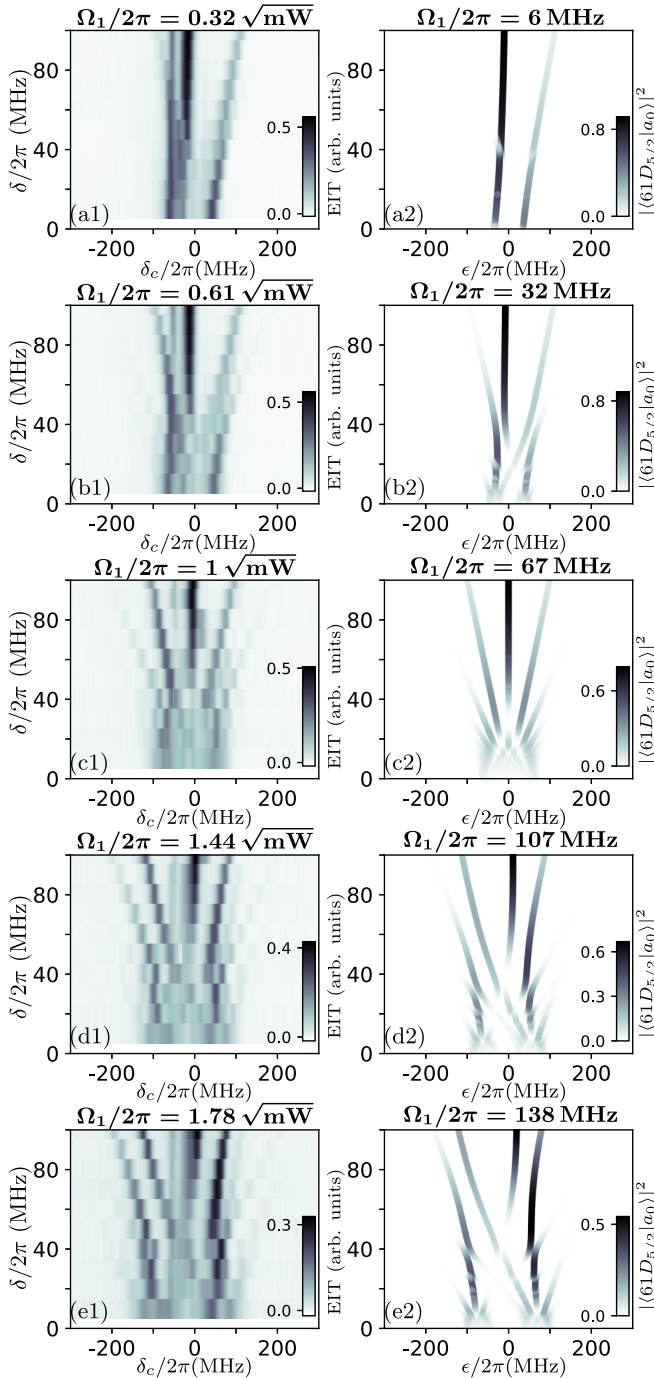


FIG. 5. (a1)–(e1) Experimental and (a2)–(e2) theoretical waterfall plots show a simultaneous scan of $\delta_1 = -\delta_2 = \delta$ while the two Rabi frequencies $|\Omega_1|$, as labeled, and $|\Omega_2| = 1\sqrt{\text{mW}}$ are kept constant. The imbalance in Rabi frequencies is apparent from the asymmetric spectra, with the shift indicating the relative Rabi strengths as the Rabi frequency $|\Omega_2|$ is larger or smaller than $|\Omega_1|$.

This is a realistic scenario, for instance, in the case where spurious signals or jamming signals are present. More complex spectra arise in this case. We make several observations of the main features of such spectra in the two-field case below.

First, when δ_2 is far off resonance, the spectrum is essentially the Autler-Townes spectrum of a single field as it sweeps

through the Rydberg resonance. The spectra are largely mirrored for the cases where the constant detuning is δ_2 vs $-\delta_2$, for example, Figs. 6(a1) and 6(g1).

Second, we mark the equal-detuning $\delta_1 = \delta_2$ case with red lines in Fig. 6. In this condition, the two frequencies match, and their combination is a single tone of arbitrary phase and amplitude due to the rf source. When the frequencies nearly match, we observe many closely spaced spectral lines when $\delta \ll \Omega$, owing to the $|J_N(\Omega/\delta)|^2$ dependence of mode occupations. We note that the theoretical model does not give the AT-split lines seen in the experimental data at the red lines since there is no residual Floquet time dependence in the microwave dressing fields, and this case would need to be computed independently.

Third, in Figs. 6(d1) and 6(d2), we have the case where $\delta_2 = 0$; that is, one field is on resonance with the Rydberg transition. The red lines thus indicate the case where both fields are on resonance. This case is interesting in that the data on either side of this red line (and with δ_1 detuned up to several tens of kHz) correspond to the atom-mixer configurations typically used to detect rf fields within a heterodyne configuration [25].

Avoided crossings appear at subharmonic resonances [marked with dashed blue lines in Fig. 6(d2)] of the Rabi frequency Ω ; when $\delta_2 = 0$, these resonances are at $\delta_1 = \pm\Omega/k$, with small shifts from these values caused by ac Stark shifts from the applied fields. In our spectra, these subharmonic resonances are further shifted due to the different generalized Rabi frequencies of our fields since the field strengths were kept equal as the detuning of a single field was scanned.

The subharmonic resonances indicate multiphoton resonances in the dual-tone dressed system, as discussed in previous experimental studies [15,18,30]. At large detunings δ_1 , the spectral lines reflect the single-field splitting of the on-resonance field, appearing at $\delta_c = \pm|\Omega_2|/2 = \pm|\Omega|/2$, marked by dashed blue vertical lines. The first subharmonic resonance, $k = 1$, occurs when the second field becomes resonant with a single-photon transition between single-field dressed states, causing a secondary splitting. The spectral structure is thus a doublet with a separation of $|\Omega_2|$ and an intradoublet splitting of $|\Omega_1|/2$. The dashed red vertical lines indicate values $\pm|\Omega_1|/4$ on either side of the $|\Omega_2|/2$ line. The second subharmonic resonance, $k = 2$, indicates a two-photon resonance between the single-field dressed states. These resonances appear at $\delta_c = \pm|\Omega_2|/2, 0$. Other subharmonic resonances with $k = 3$ and above are not easily resolved in our data. A similar investigation which appeared recently gives a closed-form expression for the splittings induced using the Jaynes-Cummings model for applications in electrometry [31].

VI. DISCUSSION AND CONCLUSION

In this work we have explored the EIT spectra of Rydberg atoms dressed with intense dual-tone rf fields. These spectra are qualitatively different from the Autler-Townes spectra of Rydberg atoms dressed with a single field. The large dipole moments of Rydberg atoms allow these effects to be investigated with modest rf powers. Our analysis validates the broad applicability of theoretical models that treat the

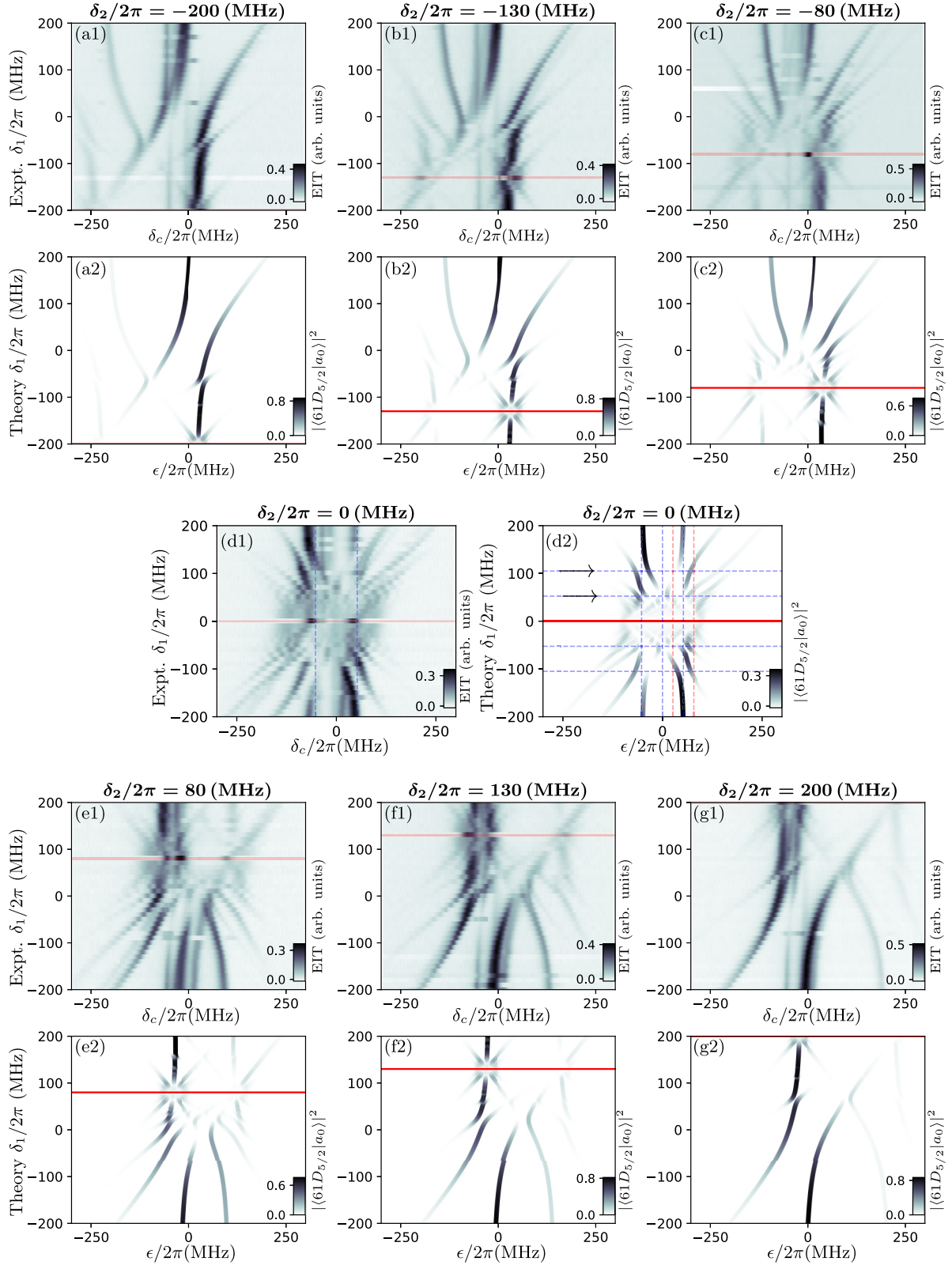


FIG. 6. (a1)–(g1) Experimental waterfall plots showing the obtained spectra against coupling laser frequency δ_c as the detuning δ_1 is scanned for constant δ_2 and Rabi frequencies $|\Omega_1| = |\Omega_2| = 105$ MHz. (a2)–(g2) Numerically obtained Floquet quasienergy spectra showing Floquet-mode occupations against quasienergies ϵ as δ_1 is scanned. The overlaid solid red lines indicate equal detunings of the two fields ($\delta_1 = \delta_2$). The arrows and overlaid dashed blue horizontal lines in (d2) indicate the first and second subharmonic resonances marked at $\delta_1 = |\Omega_2|$ and $\delta_1 = |\Omega_2|/2$. The overlaid dashed blue vertical lines in (d1) and (d2) mark $\delta_c = \pm|\Omega_2|/2$ and $\epsilon = 0, \pm|\Omega_2|/2$, respectively. The overlaid dashed red vertical lines show $\epsilon = |\Omega_2|/2 \pm |\Omega_1|/4$.

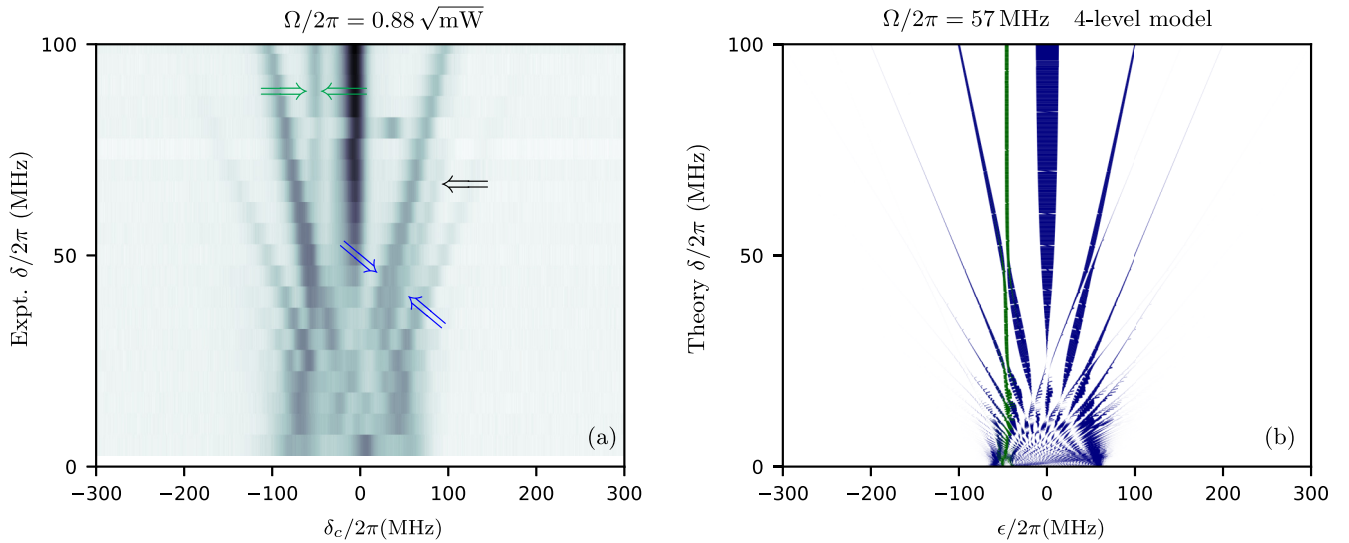


FIG. 7. The four-state model: (a) The data from Fig. 4(a1) (symmetric, power-balanced fields as the detuning is scanned) show a structure that is not accounted for in the two-level model. (b) Including the fine states in the model reproduces these features. Here, for visibility we represent the Floquet-mode occupations as the widths of the spectral lines. The overlap of the Floquet quasienergies with the zero Floquet mode of $61D_{5/2}$ is shown in blue, while the overlap with the zero Floquet mode of $61D_{3/2}$ is shown in green. We scale the initial state occupations to reflect the relative peak heights of the $61D_{3/2}$ and $61D_{5/2}$ states in order to facilitate a comparison.

two-level dynamics of the rf-dressed Rydberg levels, while the optical fields act as indirect probes of the rf-induced multiphoton dynamics. This will allow simplified treatment of dual-tone and multitone rf dressing in the Rydberg system that circumvents computationally intensive steady-state calculations with the full system density matrix. Such steady-state calculations, moreover, are nontrivial to perform in the case of dissipative systems subject to driving outside the high-frequency regime, where the interplay of driving and dissipation becomes important.

Dual-tone rf dressing of Rydberg states unlocks a different toolbox that we believe has implications for novel detection schemes in low-frequency rf field sensing. For instance, we may realize phase-sensitive detection of fields in the 100-MHz range by coupling the energy levels of the synthetic Floquet dimension with the low-frequency field to be detected, creating a three-frequency loop scheme. Previous schemes for electric-field detection in the low-frequency and dc regimes employed similar Floquet sideband techniques [32–34]. However, in those studies, the Stark shifting of energies caused field-dependent shifts of the atomic spectra, which necessitates careful calculation and retuning due to Stark shifts at the higher fields necessary to generate higher-order Floquet sidebands. In contrast, the symmetric shifts caused by symmetric dual-tone drives in the Rydberg system allow the observation of spectra in high Floquet modes without the added complication of overall spectral shifts.

One effect worth commenting on is evidenced in data and theory, where EIT spectra appear to be confined to within $\delta_c < \Omega/2$ of resonance. In the simplest form, in Fig. 2 the spectra appear in a fan-shaped spectral envelope within $\delta_c < \Omega/2$ as Ω increases up the waterfall. In Figs. 4 and 5, in waterfalls over detuning, the relative peak strengths evolve as Bessel

functions, but all peaks remain within $\approx \Omega$ of the original EIT peak.

Our work enhances our understanding of the behavior of the system in an amplitude-modulated field; in general, the symmetric dual-tone dressing may be described as a 100% sine-wave amplitude-modulated field. Amplitude modulation has been gainfully demonstrated for Rydberg-based antennas, where studies of bandwidth and sensitivity are at the forefront of research in the field. The investigations performed in this paper allow us to place on firmer footing our understanding of the response of the system to amplitude modulation and to a variety of dressing-field configurations. Our theoretical model can also be easily extended to take into account atomic structure, as we discuss in the Appendix. Further directions of inquiry include investigations of the complex atomic response in frequency-modulated driving fields, as in Refs. [30,35]. The sensitivity and accuracy of determining the amplitude and frequency selectivity of an unknown signal will be the topic of a future investigation.

Our investigations of these complex spectra will also be important as Rydberg atom-based electrometry transitions to real-world applications, where simple AT spectra may be significantly distorted and complicated by spurious tones that may be present, for example, in the case of electromagnetic signal jamming. A deeper understanding of the response of Rydberg systems to multiple tones with variable detunings and powers will be necessary in order to unravel complex real-world spectra and to obtain meaningful results.

ACKNOWLEDGMENTS

The authors would like to express their gratitude for conversations on further extensions of the theoretical model with

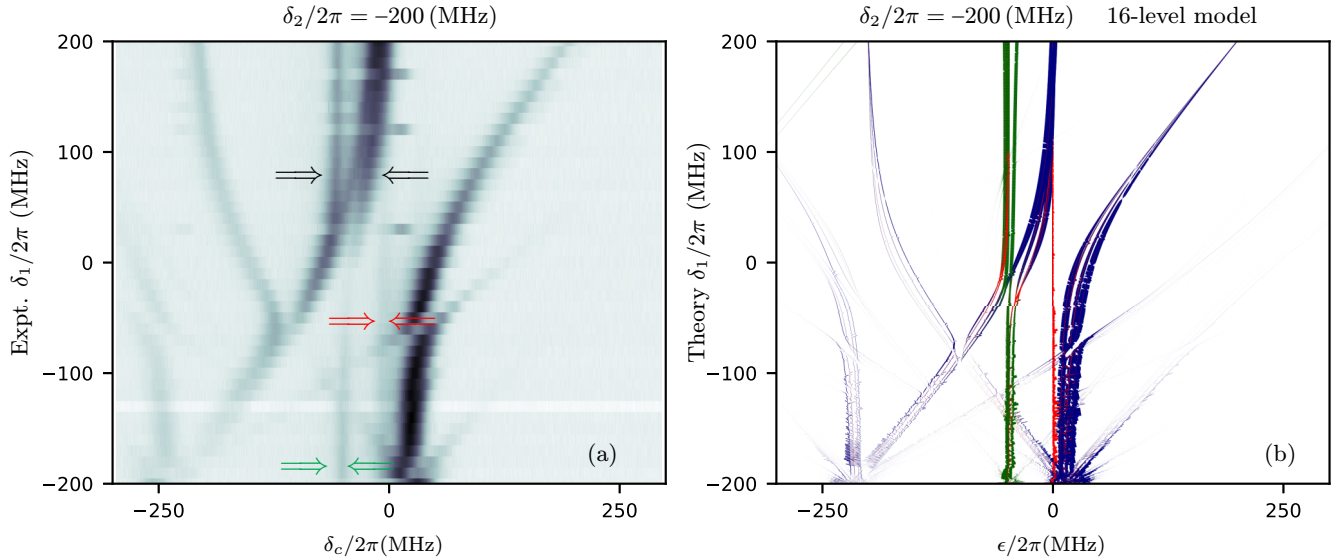


FIG. 8. The 16-state model: (a) The data from Fig. 6 (a1), with asymmetric detunings and power-balanced Rabi frequencies, as the detuning δ_1 is scanned. (b) Including the magnetic sublevels m_J of the fine states in the model reproduces more features from the data. Here, for visibility we represent the Floquet-mode occupations as the widths of the spectral lines. The overlap of the Floquet quasienergies with the $m_J = \pm 1/2$ sublevels of the zero Floquet mode of $61D_{5/2}$ is shown in navy, the overlap with the $m_J = \pm 1/2$ sublevels of the zero Floquet mode of $61D_{3/2}$ is shown in green, and other m_J components ($|m_J| > 1/2$) of both lines are shown in red. We scale the initial-state occupations of the $m_J = \pm 1/2$ components of $61D_{3/2}$ and $61D_{5/2}$ to reflect their relative peak heights from a simple EIT scan and scale the initial-state occupations of all the other m_J sublevels to be 10% of the $m_J = \pm 1/2$ occupation of $61D_{5/2}$; in general, they would depend on the polarization anisotropy and mixing of the magnetic sublevels.

R. M. Potvliege, E. L. Shirley, and S. Eckel. This work was funded by the NIST-on-a-Chip (NOAC) Program.

APPENDIX: FINE STRUCTURE AND MAGNETIC SUBLEVELS

An examination of the data in Figs. 4 and 6 shows some spectral structure that is not accounted for in our two-level model. In this Appendix we present extensions of the two-level analysis that include the fine-structure splitting of the two Rydberg states and also the magnetic sublevels of the fine-structure states.

1. Four-level model: Fine structure of Rydberg levels

We show in Fig. 7(a) the data from Fig. 4(a1), emphasizing spectral features that are not reproduced in the two-level model. In Fig. 7(b) we show results from a four-state computation that includes the states $61D_{5/2}$, $61D_{3/2}$, $62P_{3/2}$, and $62P_{1/2}$ (see Sec. A 3). The results reproduce some of the finer spectral structure that we observe in the data.

First, the green arrows in Fig. 7 highlight the appearance of the $61D_{3/2}$ fine state to the left of the zero-detuning coupling laser resonance ($\delta_c = 0$) in the EIT spectra. This feature indicates an initial population in the $61D_{3/2}$ state that does not appear to participate significantly in the dynamics. We likewise note that the $61D_{5/2}$ population does not show significant mixing into this state.

Second, the blue arrows in Fig. 7 show an apparent splitting of the spectral line due to an avoided crossing with the Floquet quasienergies associated with the fine structure. A similar avoided crossing appears on the left of the central mode.

Third, the black arrow highlights a spectral feature due to the fine structure that persists and appears more clearly for the slightly higher Rabi frequency in Fig. 4(b1): this feature is quite pronounced above the $N = 2$ mode and is absent above the $N = -2$ mode.

Fourth, an interesting feature that is not reproduced by our model is seen at quasienergies of ≈ -75 MHz in Fig. 4(b1). This is likely due to mixing from the hyperfine levels on the optical transition, which is expected to appear at this energy when Doppler mismatch is accounted for.

2. Sixteen-level model: Magnetic sublevels of Rydberg fine structure

The two-state and four-state models implicitly assume linear optical and rf polarizations. For imperfect rf polarization, faint additional lines appear in the experimental data. We confirm the locations of some of these additional features with a 16-level Hamiltonian that includes the magnetic sublevels m_J of the Rydberg fine structure (see Sec. A 3). In Fig. 8(b) we show results from a 16-state computation that includes the m_J sublevels of states $61D_{5/2}$, $61D_{3/2}$, $62P_{3/2}$, and $62P_{1/2}$. We

TABLE I. Relevant atomic energy gaps, expressed in units of frequency.

Atomic energy gaps ($1/h$)	Value
rf transition $61 D_{5/2} - 62 P_{3/2}$	9.226 GHz
Fine gap $61 D (J = 5/2 \leftrightarrow J = 3/2)$	50.339 MHz
Fine gap $62 P (J = 3/2 \leftrightarrow J = 1/2)$	415.72 MHz

TABLE II. Relevant σ^- -, π -, and σ^+ -transition dipole moments used in calculations, in atomic units of ea_0 .

Fine states	σ^- transitions ($\Delta m_J = -1$)	π transitions ($\Delta m_J = 0$)	σ^+ transitions ($\Delta m_J = +1$)
	$m_J = -3/2 \rightarrow -5/2$	$m_J = -3/2 \rightarrow -3/2$	$m_J = -3/2 \rightarrow -1/2$
$\wp_{62P_{3/2}, 61D_{5/2}}$	-3055	1932	-966
$\wp_{62P_{3/2}, 61D_{3/2}}$	0	967	-789
$\wp_{62P_{1/2}, 61D_{3/2}}$	0	0	0
	$m_J = -1/2 \rightarrow -3/2$	$m_J = -1/2 \rightarrow -1/2$	$m_J = -1/2 \rightarrow 1/2$
$\wp_{62P_{3/2}, 61D_{5/2}}$	-2366	2366	-1673
$\wp_{62P_{3/2}, 61D_{3/2}}$	789	322	-911
$\wp_{62P_{1/2}, 61D_{3/2}}$	-2765	2258	-1596
	$m_J = 1/2 \rightarrow -1/2$	$m_J = 1/2 \rightarrow 1/2$	$m_J = 1/2 \rightarrow 3/2$
$\wp_{62P_{3/2}, 61D_{5/2}}$	-1673	2366	-2366
$\wp_{62P_{3/2}, 61D_{3/2}}$	911	-322	-789
$\wp_{62P_{1/2}, 61D_{3/2}}$	-1596	2258	-2765
	$m_J = 3/2 \rightarrow 1/2$	$m_J = 3/2 \rightarrow 3/2$	$m_J = 3/2 \rightarrow 5/2$
$\wp_{62P_{3/2}, 61D_{5/2}}$	-966	1932	-3055
$\wp_{62P_{3/2}, 61D_{3/2}}$	789	-967	0
$\wp_{62P_{1/2}, 61D_{3/2}}$	0	0	0

highlight relevant features of our spectra that are reproduced in this extended model below.

First, the green arrows in Fig. 8 highlight the $61D_{3/2}$ fine state in the EIT spectra.

Second, the red arrows indicate the contamination of the Floquet quasienergy levels with $|m_J| > 1/2$ sublevels of the Rydberg states that are not accounted for in the two-state and four-state models.

Third, the complex spectra in the vicinity of the black arrows are also polarization effects that are reproduced only in the 16-state model. The mixing between the $61D_{5/2}$ and $61D_{3/2}$ states appears to take place via different m_J sublevels, as indicated by the overlap of colors in the numerical Floquet spectra in the vicinity of these features.

We note that the inclusion of the fine states and the m_J states is necessary to explain the slight asymmetry of the spectra in comparing, for instance, Figs. 6(a1) and 6(g1). As an additional point of interest, we note that the magnetic sublevels are not usually resolved in the standard Autler-Townes EIT spectra that we use for electrometry, and their behavior

in different experimental configurations contributes to our understanding of the Rydberg atomic system. A careful analysis of the relative strengths of the features that correspond to the different m_J sublevels could be used to analyze the polarization of rf fields in the spirit of previously investigated vector electrometry schemes [36].

3. Details of theoretical modeling

Here, we give further parameters used in computing the 4-level and 16-level spectra, computed using the ARC package [26].

We show the numerical values used in our calculations: here we provide energy offsets for the atomic fine-structure (Table I) and m_J -resolved dipole strengths for each available polarization (Table II).

Our Rydberg EIT spectra reflect the overlap of the Floquet modes with the bare Rydberg state $61D_{5/2}$ and state $61D_{3/2}$, which are both detected in our EIT scans.

- [1] Y. Zhu, Q. Wu, A. Lezama, D. J. Gauthier, and T. W. Mossberg, Resonance fluorescence of two-level atoms under strong bichromatic excitation, *Phys. Rev. A* **41**, 6574 (1990).
- [2] C. C. Yu, J. R. Bochinski, T. M. V. Kordich, T. W. Mossberg, and Z. Ficek, Driving the driven atom: Spectral signatures, *Phys. Rev. A* **56**, R4381 (1997).
- [3] S. Papademetriou, M. F. Van Leeuwen, and C. R. Stroud, Autler-Townes effect for an atom in a 100% amplitude-modulated laser field. II. Experimental results, *Phys. Rev. A* **53**, 997 (1996).
- [4] Q. Wu, D. J. Gauthier, and T. W. Mossberg, Phase-sensitive dynamics of bichromatically driven two-level atoms, *Phys. Rev. A* **49**, R1519 (1994).
- [5] H. Freedhoff and Z. Chen, Resonance fluorescence of a two-level atom in a strong bichromatic field, *Phys. Rev. A* **41**, 6013 (1990).
- [6] G. S. Agarwal, Y. Zhu, D. J. Gauthier, and T. W. Mossberg, Spectrum of radiation from two-level atoms under intense bichromatic excitation, *J. Opt. Soc. Am. B* **8**, 1163 (1991).
- [7] M. F. Van Leeuwen, S. Papademetriou, and C. R. Stroud, Autler-Townes effect for an atom in a 100% amplitude-modulated laser field. I. A dressed-atom approach, *Phys. Rev. A* **53**, 990 (1996).
- [8] T. G. Rudolph, Z. Ficek, and H. S. Freedhoff, The multiphoton AC Stark effect, *Opt. Commun.* **147**, 78 (1998).
- [9] S. F. Chien, M. R. B. Wahiddin, and Z. Ficek, Quantum trajectory simulations of the fluorescence intensity from a two-level atom driven by a multichromatic field, *Phys. Rev. A* **57**, 1295 (1998).
- [10] T. G. Rudolph, H. S. Freedhoff, and Z. Ficek, Multiphoton ac Stark effect in a bichromatically driven two-level atom, *Phys. Rev. A* **58**, 1296 (1998).

- [11] J. Wang, Y. Zhu, K. J. Jiang, and M. S. Zhan, Bichromatic electromagnetically induced transparency in cold rubidium atoms, *Phys. Rev. A* **68**, 063810 (2003).
- [12] H. Yan, K.-Y. Liao, J.-F. Li, Y.-X. Du, Z.-M. Zhang, and S.-L. Zhu, Bichromatic electromagnetically induced transparency in hot atomic vapors, *Phys. Rev. A* **87**, 055401 (2013).
- [13] H. Metcalf, Colloquium: Strong optical forces on atoms in multifrequency light, *Rev. Mod. Phys.* **89**, 041001 (2017).
- [14] B. Lounis, F. Jelezko, and M. Orrit, Single Molecules Driven by Strong Resonant Fields: Hyper-Raman and Subharmonic Resonances, *Phys. Rev. Lett.* **78**, 3673 (1997).
- [15] A. D. Greentree, C. Wei, S. A. Holmstrom, J. P. D. Martin, N. B. Manson, K. R. Catchpole, and C. Savage, Probing a doubly driven two-level atom, *J. Opt. B* **1**, 240 (1999).
- [16] Z. Ficek and T. Rudolph, Quantum interference in a driven two-level atom, *Phys. Rev. A* **60**, R4245 (1999).
- [17] Y. He, Y.-M. He, J. Liu, Y.-J. Wei, H. Y. Ramírez, M. Atatüre, C. Schneider, M. Kamp, S. Höfling, C.-Y. Lu, and J.-W. Pan, Dynamically Controlled Resonance Fluorescence Spectra from a Doubly Dressed Single InGaAs Quantum Dot, *Phys. Rev. Lett.* **114**, 097402 (2015).
- [18] J. Pan, Y. Fan, Y. Li, X. Dai, X. Wei, Y. Lu, C. Cao, L. Kang, W. Xu, J. Chen, G. Sun, and P. Wu, Dynamically modulated Autler-Townes effect in a transmon qubit, *Phys. Rev. B* **96**, 024502 (2017).
- [19] X.-X. Geng, K. Jin, W.-W. Tang, S. Liang, G. Yang, S.-P. Wu, G.-M. Huang, and G.-X. Li, Self-generated Floquet modulation in a multiharmonic-dressed alignment-based magnetic-resonance system, *Phys. Rev. A* **106**, 023108 (2022).
- [20] D. W. Booth, J. Isaacs, and M. Saffman, Reducing the sensitivity of Rydberg atoms to dc electric fields using two-frequency ac field dressing, *Phys. Rev. A* **97**, 012515 (2018).
- [21] A. Artusio-Glimpse, M. T. Simons, N. Prajapati, and C. L. Holloway, Modern rf measurements with hot atoms: A technology review of Rydberg atom-based radio frequency field sensors, *IEEE Microwave Mag.* **23**, 44 (2022).
- [22] K.-J. Boller, A. Imamoğlu, and S. E. Harris, Observation of Electromagnetically Induced Transparency, *Phys. Rev. Lett.* **66**, 2593 (1991).
- [23] M. Xiao, Y.-Q. Li, S.-Z. Jin, and J. Gea-Banacloche, Measurement of Dispersive Properties of Electromagnetically Induced Transparency in Rubidium Atoms, *Phys. Rev. Lett.* **74**, 666 (1995).
- [24] A. K. Mohapatra, T. R. Jackson, and C. S. Adams, Coherent Optical Detection of Highly Excited Rydberg States Using Electromagnetically Induced Transparency, *Phys. Rev. Lett.* **98**, 113003 (2007).
- [25] M. T. Simons, A. H. Haddab, J. A. Gordon, and C. L. Holloway, A Rydberg atom-based mixer: Measuring the phase of a radio frequency wave, *Appl. Phys. Lett.* **114**, 114101 (2019).
- [26] N. Šibalić, J. D. Pritchard, C. S. Adams, and K. J. Weatherill, ARC: An open-source library for calculating properties of alkali Rydberg atoms, *Comput. Phys. Commun.* **220**, 319 (2017).
- [27] P. R. Berman and V. S. Malinovsky, *Principles of Laser Spectroscopy and Quantum Optics* (Princeton University Press, Princeton, NJ, 2011).
- [28] J. H. Shirley, Solution of the Schrödinger equation with a Hamiltonian periodic in time, *Phys. Rev.* **138**, B979 (1965).
- [29] M. Tanasittikosol, J. D. Pritchard, D. Maxwell, A. Gauguier, K. J. Weatherill, R. M. Potvliege, and C. S. Adams, Microwave dressing of Rydberg dark states, *J. Phys. B* **44**, 184020 (2011).
- [30] M. W. Noel, W. M. Griffith, and T. F. Gallagher, Frequency-modulated excitation of a two-level atom, *Phys. Rev. A* **58**, 2265 (1998).
- [31] M. Noaman, D. W. Booth, and J. P. Shaffer, Rydberg-Atom Sensors in Bichromatic Radio-Frequency Fields, *Phys. Rev. Appl.* **20**, 024068 (2023).
- [32] A. P. Rotunno, S. Berweger, N. Prajapati, M. T. Simons, A. B. Artusio-Glimpse, C. L. Holloway, M. Jayaseelan, R. M. Potvliege, and C. S. Adams, Detection of HF and VHF fields through Floquet sideband gaps by ‘Rabi matching’ dressed Rydberg atoms, [arXiv:2212.03304](https://arxiv.org/abs/2212.03304).
- [33] S. A. Miller, D. A. Anderson, and G. Raithel, Radio-frequency-modulated Rydberg states in a vapor cell, *New J. Phys.* **18**, 053017 (2016).
- [34] M. G. Bason, M. Tanasittikosol, A. Sargsyan, A. K. Mohapatra, D. Sarkisyan, R. M. Potvliege, and C. S. Adams, Enhanced electric field sensitivity of rf-dressed Rydberg dark states, *New J. Phys.* **12**, 065015 (2010).
- [35] R. C. Stoneman, D. S. Thomson, and T. F. Gallagher, Microwave multiphoton transitions between Rydberg states of potassium, *Phys. Rev. A* **37**, 1527 (1988).
- [36] J. A. Sedlacek, A. Schwettmann, H. Kübler, and J. P. Shaffer, Atom-Based Vector Microwave Electrometry Using Rubidium Rydberg Atoms in a Vapor Cell, *Phys. Rev. Lett.* **111**, 063001 (2013).